

# Scalar induced gravitational waves in inflation with gravitationally enhanced friction

Chengjie Fu, Puxun Wu\* and Hongwei Yu

*Department of Physics and Synergetic Innovation*

*Center for Quantum Effects and Applications,*

*Hunan Normal University, Changsha, Hunan 410081, China*

## Abstract

We study the scalar induced gravitational wave (GW) background in inflation with gravitationally enhanced friction (GEF). The GEF mechanism, which is realized by assuming a nonminimal derivative coupling between the inflaton field and gravity, is used to amplify the small-scale curvature perturbations to generate a sizable amount of primordial black holes. We find that the GW energy spectra can reach the detectable scopes of the future GW projects, and the power spectrum of curvature perturbations has a power-law form in the vicinity of the peak. The scaling of the GW spectrum in the ultraviolet regions is two times that of the power spectrum slope, and has a lower bound. In the infrared regions, the slope of the GW spectrum can be described roughly by a log-dependent form. These features of the GW spectrum may be used to check the GEF mechanism if the scalar induced GWs are detected in the future.

---

\* Corresponding author: pxwu@hunnu.edu.cn

## I. INTRODUCTION

Primordial black holes (PBHs) may be formed in the very early era of the universe. Their implications on the astronomy and cosmology have recently been receiving extensive attention. It has been pointed out that PBHs can be taken as the possible sources of some astronomical events, on one hand. For example, the stellar-mass ( $\sim \mathcal{O}(10)M_\odot$ ) PBHs are considered to be the promising candidate responsible for some gravitational wave (GW) events [1–3], which are radiated by the binary BH mergers and have been detected by the LIGO-Virgo Collaboration [4]. PBHs with earth mass ( $\sim \mathcal{O}(10^{-5})M_\odot$ ) can account for six ultrashort-timescale microlensing events in the 5-year OGLE dataset [5, 6]. In addition, an earth mass PBH, if it is captured by the Solar System, has been used to explain the anomalous orbits of Trans-Neptunian Objects [7]. On the other hand, PBHs have also been proposed as the candidate of dark matter, and they have a possibility for making up all dark matter in two asteroid-mass intervals:  $\mathcal{O}(10^{-16}) \sim (10^{-14})M_\odot$  and  $\mathcal{O}(10^{-13}) \sim (10^{-11})M_\odot$  [8, 9].

The PBH formation requires that the primordial curvature perturbations produced during the inflation era, which seed the large-scale structure of the Universe, have a suitably large amplitude. Since the cosmic microwave background (CMB) observations have constrained the curvature perturbations to have an amplitude about  $10^{-5}$  [10] at the CMB (large) scale, in order to generate a sizable amount of PBHs we need to enhance the small-scale curvature perturbations during inflation. When these enhanced curvature perturbations re-enter the horizon, they will result in the formation of black holes in the overdensed regions, and, at the same time, lead to very large scalar metric perturbations. These scalar perturbations couple with the tensor perturbations at the second order, although they decouple with each other at the linear level. Inevitably, the large scalar metric perturbations will become a significant GW source and generate abundant GW signals via the second-order effect to form the stochastic GW background [11–18]. Therefore, detecting the concomitant induced GW signals provides an inspiring possibility and a whole new way to search for the existence of PBHs.

The mechanisms of amplifying the small-scale curvature perturbations within the inflationary scenario have been extensively studied in recent years [19–34]. The most common mechanism is the single-field inflection-point inflation [27–34], which requires that the po-

tential of the inflaton field has an approximate inflection point. The rolling of the inflaton decelerates when it comes close to the inflection point. As a result, the Universe experiences a period of ultra-slow-roll inflation in the vicinity of the inflection point, which enhances the curvature perturbations.

Recently, a novel enhancement mechanism of curvature perturbations was proposed by us in [35], in which the velocity of inflaton is decreased by the increased friction. To enhance the friction, we consider a nonminimal derivative coupling between the inflation field and gravity with the action being

$$\mathcal{S} = \int d^4x \sqrt{-g} \left[ \frac{1}{2\kappa^2} R - \frac{1}{2} (g^{\mu\nu} - \kappa^2 \theta(\phi) G^{\mu\nu}) \nabla_\mu \phi \nabla_\nu \phi - V(\phi) \right], \quad (1)$$

where  $\kappa^{-1} \equiv M_{\text{pl}} = 2.4 \times 10^{18}$  GeV is the reduced Planck mass,  $g$  the determinant of the metric tensor  $g_{\mu\nu}$ ,  $R$  the Ricci scalar,  $G^{\mu\nu}$  the Einstein tensor,  $\theta$  a dimensionless coupling parameter, which is function of  $\phi$ , and  $V(\phi)$  the potential of the inflaton field. By choosing a special function form of  $\theta(\phi)$ , i.e.  $\theta = \omega / \sqrt{\kappa^2 \left( \frac{\phi - \phi_c}{\sigma} \right)^2 + 1}$ , a high-friction region can be realized at the slow-roll stage through the mechanism of the gravitationally enhanced friction (GEF). Here,  $\omega$ ,  $\sigma$  and  $\phi_c$  are constants. Thus, when the inflaton goes through this region, it experiences an extremely slow speed. The amplitude of the curvature perturbations is amplified during this ultra-slow-roll inflation era. In Ref. [35], we demonstrated that PBHs with physically attractive masses, such as  $\mathcal{O}(10)M_\odot$ ,  $\mathcal{O}(10^{-5})M_\odot$ ,  $\mathcal{O}(10^{-12})M_\odot$ , can be generated as a result of the amplified curvature perturbations by the GEF mechanism.

The PBH formation is accompanied inevitably with the production of significant GW backgrounds induced by the overly large curvature perturbations. The detection of such GW signals may serve as evidence of the GEF mechanism. This motivates us to carry out the investigation in the present paper, that is to perform a comprehensive analysis on the scalar induced GWs in the inflation model with a nonminimal derivative coupling. We organize our paper as follows: In Sec. II, we outline the basic formulas about the second-order GWs and calculate the GW energy spectra associated with the PHB formation studied in Ref. [35]. In Sec. III, we analyze the scaling of the scalar induced GW spectra. Section IV gives our conclusions. In addition, the main equations of the nonminimal derivative coupling inflation model are outlined in the Appendix.

## II. GRAVITATIONAL WAVES INDUCED BY CURVATURE PERTURBATIONS

We first give the basic formulas for scalar induced GWs through the second-order effect of the curvature perturbations. Ignoring the anisotropic stress, the perturbed Friedmann-Robertson-Walker (FRW) metric in the conformal Newtonian gauge has the form [36]

$$ds^2 = a(\eta)^2 \left\{ -(1 + 2\Psi)d\eta^2 + \left[ (1 - 2\Psi)\delta_{ij} + \frac{h_{ij}}{2} \right] dx^i dx^j \right\} , \quad (2)$$

where  $a$  is the cosmic scale factor,  $\eta \equiv \int a^{-1} dt$  is the conformal time,  $\Psi$  is the first-order scalar perturbation, and  $h_{ij}$  represents the second-order transverse-traceless tensor perturbation.

At the second order, the equation of motion for  $h_{ij}$  can be derived from the Einstein equation

$$h''_{ij} + 2\mathcal{H}h'_{ij} - \nabla^2 h_{ij} = -4\mathcal{T}_{ij}^{lm} S_{lm} , \quad (3)$$

where a prime denotes the derivative with respect to the conformal time and  $\mathcal{H} \equiv a'/a$  is the conformal Hubble parameter. Here  $\mathcal{T}_{ij}^{lm}$  is the transverse-traceless projection operator and  $S_{ij}$  is the GW source term [36, 37]

$$S_{ij} = 4\Psi\partial_i\partial_j\Psi + 2\partial_i\Psi\partial_j\Psi - \frac{1}{\mathcal{H}^2}\partial_i(\mathcal{H}\Psi + \Psi')\partial_j(\mathcal{H}\Psi + \Psi') . \quad (4)$$

At the radiation-dominated era, the scalar metric perturbation  $\Psi$  in the Fourier space satisfies the equation

$$\Psi''_k + \frac{4}{\eta}\Psi'_k + \frac{k^2}{3}\Psi_k = 0 , \quad (5)$$

which admits a solution [37]

$$\Psi_k(\eta) = \psi_k \frac{9}{(k\eta)^2} \left( \frac{\sin(k\eta/\sqrt{3})}{k\eta/\sqrt{3}} - \cos(k\eta/\sqrt{3}) \right) , \quad (6)$$

where  $k$  is the comoving wave number, and  $\psi_k$  is the primordial perturbation, which relates to the power spectrum of the curvature perturbation through

$$\langle \psi_{\mathbf{k}} \psi_{\tilde{\mathbf{k}}} \rangle = \frac{2\pi^2}{k^3} \left( \frac{4}{9} \mathcal{P}_{\mathcal{R}}(k) \right) \delta(\mathbf{k} + \tilde{\mathbf{k}}) . \quad (7)$$

During the radiation-dominated era, the energy density of the scalar induced GWs per logarithmic interval of  $k$  can be evaluated as [11]

$$\Omega_{\text{GW}}(\eta_c, k) = \frac{1}{12} \int_0^\infty dv \int_{|1-v|}^{|1+v|} du \left( \frac{4v^2 - (1 + v^2 - u^2)^2}{4uv} \right)^2 \mathcal{P}_{\mathcal{R}}(ku) \mathcal{P}_{\mathcal{R}}(kv) \\ \left( \frac{3}{4u^3v^3} \right)^2 (u^2 + v^2 - 3)^2 \\ \left\{ \left[ -4uv + (u^2 + v^2 - 3) \ln \left| \frac{3 - (u+v)^2}{3 - (u-v)^2} \right| \right]^2 + \pi^2 (u^2 + v^2 - 3)^2 \Theta(v + u - \sqrt{3}) \right\} \quad (8)$$

at time  $\eta_c$ , which represents the time when  $\Omega_{\text{GW}}$  stops to grow. Here  $\Theta$  is the Heaviside theta function. Between the energy spectra of the induced GWs at present and at  $\eta_c$  there exists a relation [14]

$$\Omega_{\text{GW},0} = 0.83 \left( \frac{g_c}{10.75} \right)^{-1/3} \Omega_{\text{r},0} \Omega_{\text{GW}}(\eta_c, k), \quad (9)$$

where  $\Omega_{\text{r},0} \simeq 4.2 \times 10^{-5}$  is the current density parameter of radiation. Here  $g_c \simeq 106.75$  denotes the effective degrees of freedom in the energy density at  $\eta_c$ . The current frequency  $f$  of the scalar induced GWs relates with the comoving wave number  $k$  through the following equation

$$f = 1.546 \times 10^{-15} \frac{k}{\text{Mpc}^{-1}} \text{Hz}. \quad (10)$$

Integrating Eq. (8) numerically and using Eqs. (9, 10), one can obtain the predicted current energy spectra of the scalar induced GWs associated with the production of PBHs. The results are shown in Fig. 1, in which the solid, dashed and dotted curves correspond to the PBHs with asteroid-mass, earth-mass, and stellar-mass, respectively. Apparently, the GW spectra have almost the same shape and amplitude, but different peak frequencies. The smaller the mass of PBHs, the higher the peak frequency of the GW spectrum has. In the case of asteroid-mass PBHs, the peak of the GW spectrum locates in the sensitive region of LISA and the high-frequency part of the GW spectrum exceeds the sensitivity curves of DECIGO and BBO. The low- and high-frequency parts of the GW spectrum related to the earth-mass PBH formation are above sensitivities of SKA and LISA respectively. However, the dotted curve indicates that the scalar induced GW spectrum associated with the stellar-mass BH generation crosses the regions excluded by EPTA, although the curvature perturbations generating stellar-mass PBHs meet the EPTA constraint [35]. This

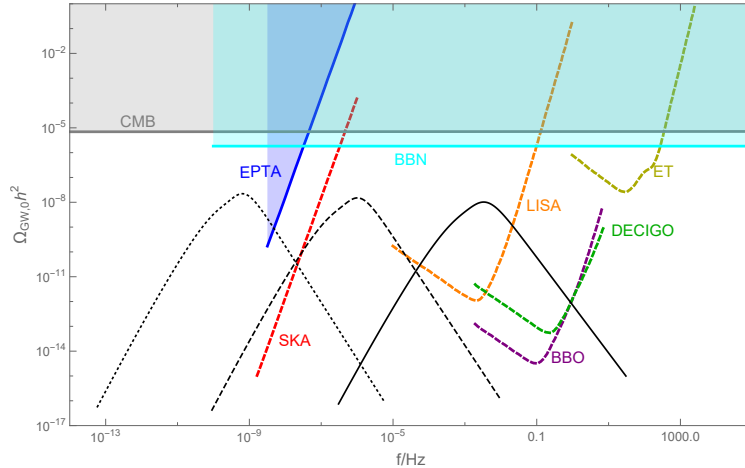


FIG. 1: The current energy spectra of the induced GWs predicted by our model (black line). The solid/dashed/dotted black lines correspond to the production of asteroid-mass, earth-mass, and stellar-mass PBHs, respectively. The shaded regions represent the existing constraints on GWs from CMB [38], BBN [11], and EPTA [39]. The other dashed lines are the expected sensitivity curve of the future gravitational-wave projects summarized in [40].

constraint is obtained conservatively by parametrizing the power spectrum of curvature perturbations [14]. In [35], the Press-Schechter approach with the Gaussian window function has been used to discuss the production rate of PBHs. It has been pointed in Ref. [25] that if one adopts the Press-Schechter approach with the real-space top-hat window function instead of the Gaussian window function or the refined peak-theory approach [41] to calculate the abundance of PBHs, the required curvature perturbations are relatively smaller and then the corresponding GWs are consistent with the current EPTA constraint. Thus, we guess that the scalar induced GW from the GEF mechanism can also be consistent with the EPTA if the real-space top-hat window function or the refined peak-theory approach is adopted. Besides the scalar induced GW spectra, another important quantity is the scaling of the GWs since it is crucial to distinguishing different mechanisms for the generation of large primordial curvature perturbations.

### III. SCALING OF SCALAR INDUCED GRAVITATIONAL WAVES

Since the shape of scalar induced GW spectra relates to the scaling of the power spectrum of curvature perturbations, we first derive the slope of the power spectrum in the

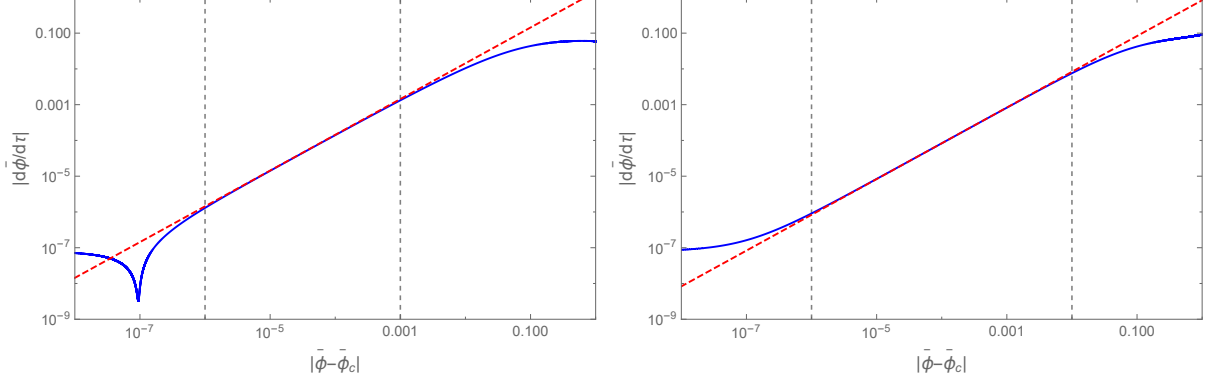


FIG. 2: The evolution of  $|d\bar{\phi}/d\tau|$  as a function of  $|\bar{\phi} - \bar{\phi}_c|$  when  $\bar{\phi} > \bar{\phi}_c$  (left panel) and  $\bar{\phi} < \bar{\phi}_c$  (right panel). The parameters are set for the earth-mass PBH generation (the second row of Tab. (I) in Appendix). The blue solid lines represent the results by solving numerically equations and the red dashed lines are our analytical results given in Eq. (16).

vicinity of the peak analytically and compare the analytical result with that from numerically solving the Mukhanov-Sasaki equation. After introducing a dimensionless time variable  $\tau \equiv \sqrt{\lambda}\kappa^{-1}t$ , where  $\lambda$  is a dimensionless parameter in the inflationary potential (A6), and a dimensionless field  $\bar{\phi} \equiv \kappa\phi$ , the Friedmann equation and the dynamical equation of the inflaton field given in Eqs. (A12) and (A14) can be re-expressed as

$$3\bar{H}^2 \simeq \bar{\phi}^{2/5}, \quad (11)$$

$$\left(1 + 3\bar{\theta}(\bar{\phi})\bar{H}^2\right)\frac{d^2\bar{\phi}}{d\tau^2} + \left(1 + 3\bar{\theta}(\bar{\phi})\bar{H}^2\right)3\bar{H}\frac{d\bar{\phi}}{d\tau} + \frac{3}{2}\bar{\theta}_{,\bar{\phi}}\bar{H}^2\left(\frac{d\bar{\phi}}{d\tau}\right)^2 + \frac{2}{5}\bar{\phi}^{-3/5} \simeq 0, \quad (12)$$

where  $\bar{H} \equiv (da/d\tau)a^{-1}$ ,  $\bar{\theta}(\bar{\phi}) = \lambda\theta(\bar{\phi})$  and  $\bar{\theta}_{,\bar{\phi}} = d\bar{\theta}/d\bar{\phi}$  have the following forms

$$\bar{\theta} = \frac{\sigma\omega\lambda}{\sqrt{(\bar{\phi} - \bar{\phi}_c)^2 + \sigma^2}}, \quad \bar{\theta}_{,\bar{\phi}} = -\frac{\sigma\omega\lambda(\bar{\phi} - \bar{\phi}_c)}{[(\bar{\phi} - \bar{\phi}_c)^2 + \sigma^2]^{3/2}}. \quad (13)$$

Since the value of  $\sigma$  ( $\sim 10^{-9}$ ) is very very small, the value of  $|\bar{\phi} - \bar{\phi}_c|$  is usually much larger than that of  $\sigma$  except for the regions where  $\bar{\phi}$  is extremely close to  $\bar{\phi}_c$ . So, we can investigate the ultra-slow-roll inflationary dynamics under the condition  $\sigma \ll |\bar{\phi} - \bar{\phi}_c|$ . In this case  $\bar{\theta}$  and  $\bar{\theta}_{,\bar{\phi}}$  can be simplified to be

$$\bar{\theta} \simeq \begin{cases} +\frac{\sigma\omega\lambda}{\bar{\phi} - \bar{\phi}_c}, & (\bar{\phi} > \bar{\phi}_c) \\ -\frac{\sigma\omega\lambda}{\bar{\phi} - \bar{\phi}_c}, & (\bar{\phi} < \bar{\phi}_c) \end{cases}, \quad \bar{\theta}_{,\bar{\phi}} \simeq \begin{cases} -\frac{\sigma\omega\lambda}{(\bar{\phi} - \bar{\phi}_c)^2}, & (\bar{\phi} > \bar{\phi}_c) \\ +\frac{\sigma\omega\lambda}{(\bar{\phi} - \bar{\phi}_c)^2}, & (\bar{\phi} < \bar{\phi}_c) \end{cases}. \quad (14)$$

In Eq. (12), the second term in the left hand side is the friction term arising from the derivative coupling and the cosmic expansion. As discussed in Ref. [35], the strong friction condition  $\bar{\theta}(\bar{\phi})\bar{H}^2 \gg 1$  can be satisfied easily in the vicinity of  $\phi_c$ . In addition,  $\bar{H} \simeq \bar{\phi}_c^{1/5}/\sqrt{3}$  is almost a constant in the vicinity of  $\phi_c$ . Thus, during the ultra-slow-roll era Eq. (12) reduces to

$$\begin{aligned} \frac{\sigma\omega\lambda}{\bar{\phi}-\bar{\phi}_c} \frac{d^2\bar{\phi}}{d\tau^2} + \sqrt{3}\bar{\phi}_c^{1/5} \frac{\sigma\omega\lambda}{\bar{\phi}-\bar{\phi}_c} \frac{d\bar{\phi}}{d\tau} - \frac{1}{2} \frac{\sigma\omega\lambda}{(\bar{\phi}-\bar{\phi}_c)^2} \left( \frac{d\bar{\phi}}{d\tau} \right)^2 + \frac{2}{5}\bar{\phi}_c^{-1} &\simeq 0, \text{ for } \bar{\phi} > \bar{\phi}_c, \\ -\frac{\sigma\omega\lambda}{\bar{\phi}-\bar{\phi}_c} \frac{d^2\bar{\phi}}{d\tau^2} - \sqrt{3}\bar{\phi}_c^{1/5} \frac{\sigma\omega\lambda}{\bar{\phi}-\bar{\phi}_c} \frac{d\bar{\phi}}{d\tau} + \frac{1}{2} \frac{\sigma\omega\lambda}{(\bar{\phi}-\bar{\phi}_c)^2} \left( \frac{d\bar{\phi}}{d\tau} \right)^2 + \frac{2}{5}\bar{\phi}_c^{-1} &\simeq 0, \text{ for } \bar{\phi} < \bar{\phi}_c. \end{aligned} \quad (15)$$

This equation has a linear solution:

$$\frac{d\bar{\phi}}{d\tau} \simeq \begin{cases} \sqrt{3}\bar{\phi}_c^{1/5} \left( \sqrt{1 - \frac{4}{15}\bar{\phi}_c^{-7/5}(\sigma\omega\lambda)^{-1}} - 1 \right) (\bar{\phi} - \bar{\phi}_c), & (\bar{\phi} > \bar{\phi}_c) \\ \sqrt{3}\bar{\phi}_c^{1/5} \left( \sqrt{1 + \frac{4}{15}\bar{\phi}_c^{-7/5}(\sigma\omega\lambda)^{-1}} - 1 \right) (\bar{\phi} - \bar{\phi}_c), & (\bar{\phi} < \bar{\phi}_c) \end{cases}. \quad (16)$$

Figure 2 shows the evolution of  $|d\bar{\phi}/d\tau|$  as a function of  $|\bar{\phi} - \bar{\phi}_c|$  with the parameters set for the earth-mass PBH generation (the second row of Tab. (I) in Appendix), which also serves as an concrete example in the subsequent numerical calculation used to test our analytic results. From this figure, one can see that the relations between  $d\bar{\phi}/d\tau$  and  $(\bar{\phi} - \bar{\phi}_c)$  given in Eq. (16) are nicely consistent with the numerical results.

During the ultra-slow-roll era which is resulted from the GEF ( $\bar{\theta}(\bar{\phi})\bar{H}^2 \gg 1$ ), the slow-roll conditions  $\delta_X$  and  $\delta_D$  defined in (A4) satisfy  $\delta_D \ll \delta_X$ . So, Eq. (A16) indicates that the power spectrum of curvature perturbations  $\mathcal{P}_{\mathcal{R}}$  is inversely proportional to  $\delta_D$ . Using Eq. (14, 16), one can obtain  $\mathcal{P}_{\mathcal{R}} \propto (\bar{\phi} - \bar{\phi}_c)^{-1}$ . Since the tilt of the power spectrum is calculated to be

$$\frac{d \ln \mathcal{P}_{\mathcal{R}}}{d \ln k} = \left( \frac{d \ln \mathcal{P}_{\mathcal{R}}}{dt} \right) \left( \frac{dt}{d \ln(aH)} \right) \simeq -\frac{1}{\bar{H}(\bar{\phi} - \bar{\phi}_c)} \frac{d\bar{\phi}}{d\tau}, \quad (17)$$

we obtain a power-law power spectrum for the curvature perturbations

$$\mathcal{P}_{\mathcal{R}} \simeq \begin{cases} k^{n_1}, & (k < k_p) \\ k^{n_2}, & (k > k_p) \end{cases} \quad (18)$$



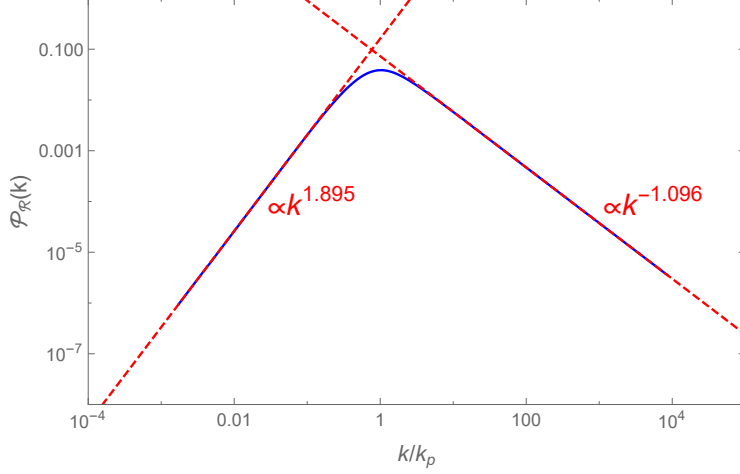


FIG. 3: The power spectrum of curvature perturbations versus  $k/k_p$  with the parameters chosen to be the second row of Tab. (I) in Appendix. The blue solid line is the power spectrum obtained by solving numerically the Mukhanov-Sasaki equation. Two red dashed lines have the slopes of  $k^{1.895}$  and  $k^{-1.096}$  as the analytic prediction given in Eq. (18) .

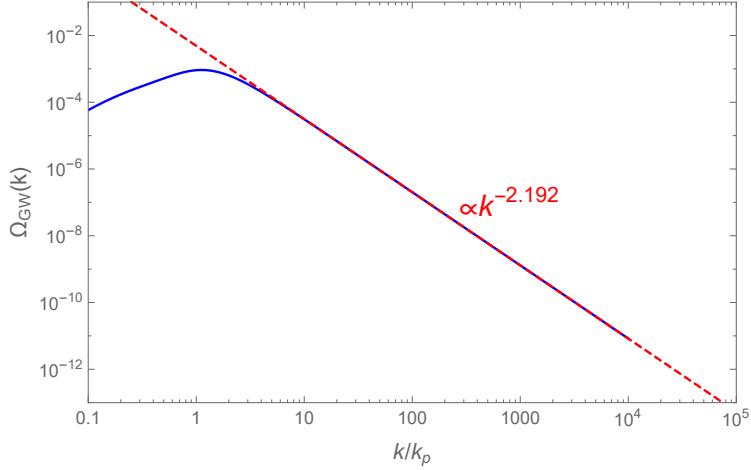


FIG. 4: The energy spectrum of the induced GWs as a function of  $k/k_p$  at  $\eta_c$ . The parameters are set to be the same as those in Fig. (3). The solid blue line is the numerical result, and the dashed red line corresponds to the analytic result  $\Omega_{\text{GW}} \propto k^{-2.192}$ .

by using Eq. (16). Here, the spectral indexes take the forms

$$\begin{aligned} n_1 &= 3 \left( 1 - \sqrt{1 - \frac{4}{15} (\kappa \phi_c)^{-7/5} (\sigma \omega \lambda)^{-1}} \right) , \\ n_2 &= 3 \left( 1 - \sqrt{1 + \frac{4}{15} (\kappa \phi_c)^{-7/5} (\sigma \omega \lambda)^{-1}} \right) . \end{aligned} \quad (19)$$

and  $k_p$  represents the comoving wave number corresponding to the peak of the power spec-

trum. The power spectra given in Eq. (18) and that obtained by numerically solving the Mukhanov-Sasaki equation (A7) are compared in Fig. 3, from which one can see that the power spectrum in our model can be well modeled by a power law with the slopes being  $n_1$  and  $n_2$  in the vicinity of peak. We must point out that the expression of  $n_1$  given in Eq. (19) is valid only when  $4(\kappa\phi_c)^{-7/5}(\sigma\omega\lambda)^{-1} \lesssim 15$ . Actually, numerical calculations indicate that if  $4(\kappa\phi_c)^{-7/5}(\sigma\omega\lambda)^{-1} > 15$ , our mechanism of enhancing the curvature perturbations will become inefficient and the amplitude of the power spectrum cannot grow up to reach the typical value expected to generate a sufficient abundance of PBHs. As a result, we give a rough bound on the slope of power spectrum with  $n_1 \lesssim 3$  and  $n_2 \gtrsim -1.24$ .

A comparison of figures 4 and 3 reveals that in the ultraviolet regions ( $k \gg k_p$ ) the power-law behavior of the scalar induced GWs has a slope  $n_{\text{GW}} \simeq 2n_2$ , which is consistent with the result given in Ref. [17] where it was found that if the power spectrum has the form  $\mathcal{P}_{\mathcal{R}} \propto k^n$  with  $n > -4$  the induced GW spectra have a  $k^{2n}$  slope when  $k \gg k_p$ . Due to  $n_2 \gtrsim -1.24$ , the slope of the induced GWs is roughly limited to be  $n_{\text{GW}} \gtrsim -2.48$  in the ultraviolet regions. However, in the infrared regions ( $k \ll k_p$ ), we do not find a simple relation between the slopes of the induced GW spectrum and the power spectrum of curvature perturbations. But, in [42] Yuan et al. found an approximate log-dependent slope of the GWs induced by scalar curvature perturbations

$$n_{\text{GW}} = 3 - \frac{4}{\ln \frac{4k_p^2}{3k^2}}. \quad (20)$$

In Fig. 5, we plot the relative error of  $n_{\text{GW}}$  for the model considered in the present paper by comparing the approximate and numerical results. The error becomes smaller and smaller with the decrease of  $k/k_p$ . When  $k/k_p \lesssim 2 \times 10^{-3}$  the relative error decreases to be less than 5%, which indicates that such a log-dependent slope can describe roughly the infrared behavior of the GW spectrum for the model with the gravitationally enhanced curvature perturbations.

#### IV. CONCLUSIONS

We have recently proposed a GEF mechanism to amplify the amplitude of curvature perturbations at small scales and then found that a sizable amount of PBHs can be generated [35]. Following this work, we here further discuss the production of the GWs induced by

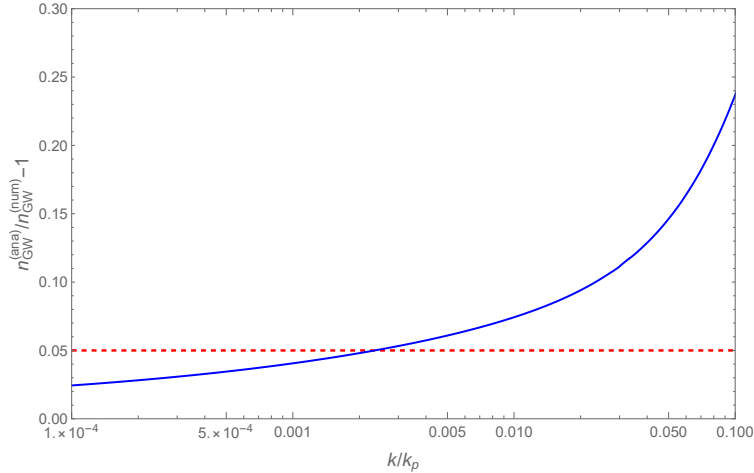


FIG. 5: The relative error of  $n_{\text{GW}}$  as a function of  $k/k_p$ .  $n_{\text{GW}}^{(\text{ana})}$  is the analytic result given in Eq. (20) and  $n_{\text{GW}}^{(\text{num})}$  is the numerical one. The parameters are set to be the same as those in Fig. (3).

the enhanced curvature perturbations in this paper. We consider three typical GW spectra associated with the formation of PBHs with the mass around  $\mathcal{O}(10)M_\odot$ ,  $\mathcal{O}(10^{-5})M_\odot$  and  $\mathcal{O}(10^{-12})M_\odot$ , respectively. We find that the GW signals induced by the curvature perturbations can be probed by the future GW experiments. However, the energy spectrum of GWs, which relates to the stellar-mass PBH production estimated by using the Press-Schechter approach with the Gaussian window function, fails to satisfy the current constraint from EPTA. Our result is in agreement with what was obtained in [25], and moreover, the authors there also point out that once the Press-Schechter approach with the real-space top-hat window function or the refined peak-theory approach to calculate the abundance of PBHs is adopted, the required curvature perturbations are relatively smaller and then the corresponding GWs will be consistent with the current EPTA constraint. Thus, we guess that the incompatibility between the predicted GWs from GEF mechanism and the EPTA observation can also be avoided by using the real-space top-hat window function or the refined peak-theory approach for the PBH production. Furthermore, we examine the scaling of the power spectrum of curvature perturbations and the scalar induced GW spectrum. We find that, in the vicinity of peak, the power spectrum has a power-law form. In the ultraviolet regions, the scaling of the GW spectrum is two times that of the power spectrum slope, and has a lower bound. While, in the infrared regions, the slope of the GW spectrum can only be described roughly by a log-dependent form. These features of the GW spectrum from the amplified curvature perturbations may be used to check the GEF mechanism if the scalar

induced GWs are successfully detected in the future.

### Acknowledgments

We thank Jing Liu very much for fruitful discussions. This work was supported by the National Natural Science Foundation of China under Grants No. 11775077, No. 11435006, and No. 11690034, and by the Science and Technology Innovation Plan of Hunan province under Grant No. 2017XK2019.

### Appendix A: Main formulas of inflation model with a nonminimal derivative coupling

From the action (1), we derive the following equations in the spatially flat FRW background,

$$3H^2 = \kappa^2 \left[ \frac{1}{2} \left( 1 + 9\kappa^2 \theta(\phi) H^2 \right) \dot{\phi}^2 + V(\phi) \right] , \quad (\text{A1})$$

$$-2\dot{H} = \kappa^2 \left[ \left( 1 + 3\kappa^2 \theta(\phi) H^2 - \kappa^2 \theta(\phi) \dot{H} \right) \dot{\phi}^2 - \kappa^2 \theta_{,\phi} H \dot{\phi}^3 - 2\kappa^2 \theta(\phi) H \dot{\phi} \ddot{\phi} \right] , \quad (\text{A2})$$

$$\left( 1 + 3\kappa^2 \theta(\phi) H^2 \right) \ddot{\phi} + \left[ 1 + \kappa^2 \theta(\phi) \left( 2\dot{H} + 3H^2 \right) \right] 3H\dot{\phi} + \frac{3}{2} \kappa^2 \theta_{,\phi} H^2 \dot{\phi}^2 + V_{,\phi} = 0 , \quad (\text{A3})$$

where  $\theta_{,\phi} = d\theta/d\phi$ ,  $V_{,\phi} = dV/d\phi$ ,  $H \equiv \dot{a}/a$  is the Hubble parameter and a dot denotes the derivative with respect to the cosmic time. The slow-roll inflation is characterized by

$$\epsilon \equiv -\frac{\dot{H}}{H^2} \ll 1 , \quad \delta_\phi \equiv \left| \frac{\ddot{\phi}}{H\dot{\phi}} \right| \ll 1 , \quad \delta_X \equiv \frac{\kappa^2 \dot{\phi}^2}{2H^2} \ll 1 , \quad \delta_D \equiv \frac{\kappa^4 \theta \dot{\phi}^2}{4} \ll 1 . \quad (\text{A4})$$

In Ref. [35], we consider a special functional form of  $\theta(\phi)$

$$\theta = \frac{\omega}{\sqrt{\kappa^2 \left( \frac{\phi - \phi_c}{\sigma} \right)^2 + 1}} , \quad (\text{A5})$$

and a fractional power-law potential

$$V = \lambda M_{\text{pl}}^{18/5} |\phi|^{2/5} , \quad (\text{A6})$$

#	$\phi_c/M_{\text{pl}}$	$\omega\lambda$	$\sigma$
$\sim \mathcal{O}(10)M_\odot$	4.63	$1.33 \times 10^7$	$2.6 \times 10^{-9}$
$\sim \mathcal{O}(10^{-5})M_\odot$	3.9	$1.53 \times 10^7$	$3 \times 10^{-9}$
$\sim \mathcal{O}(10^{-12})M_\odot$	3.3	$1.978 \times 10^7$	$3.4 \times 10^{-9}$

TABLE I: The three parameter sets considered in Ref. [35].

where  $\lambda$ ,  $\omega$  and  $\sigma$  are dimensionless parameters, and  $\phi_c$  has the dimension of mass. Table I gives the choices of these parameters for successfully generating the stellar-mass, earth-mass, and asteroid-mass PBHs.

The Mukhanov-Sasaki equation is given by

$$u_k'' + \left( c_s^2 k^2 - \frac{z''}{z} \right) u_k = 0, \quad (\text{A7})$$

where  $z \equiv \sqrt{2Q_s}a$  and  $u \equiv z\mathcal{R}$ . Note that  $\mathcal{R}$  is the comoving curvature perturbation,  $Q_s$  and  $c_s^2$  have the following forms

$$Q_s = \frac{w_1(4w_1w_3 + 9w_2^2)}{3w_2^2}, \quad (\text{A8})$$

$$c_s^2 = \frac{3(2w_1^2w_2H - w_2^2w_4 + 4w_1\dot{w}_1w_2 - 2w_1^2\dot{w}_2)}{w_1(4w_1w_3 + 9w_2^2)}, \quad (\text{A9})$$

with

$$\begin{aligned} w_1 &= M_{\text{pl}}^2(1 - 2\delta_D), \\ w_2 &= 2HM_{\text{pl}}^2(1 - 6\delta_D), \\ w_3 &= -3H^2M_{\text{pl}}^2(3 - \delta_X - 36\delta_D), \\ w_4 &= M_{\text{pl}}^2(1 + 2\delta_D). \end{aligned} \quad (\text{A10})$$

The power spectrum of curvature perturbations can be calculated as

$$\mathcal{P}_{\mathcal{R}} = \frac{k^3}{2\pi^2} \left| \frac{u_k}{z} \right|^2 = \frac{H^2}{8\pi^2 Q_s c_s^3}. \quad (\text{A11})$$

As we have pointed out in Ref. [35], although the slow-roll condition  $\delta_\phi \ll 1$  is violated at the period of ultra-slow-roll inflation, other slow-roll conditions  $\{\epsilon, \delta_X, \delta_D\} \ll 1$  are valid. Thus, during the inflationary phase, Eqs. (A1)-(A3) can always be simplified, respectively, to be

$$3H^2 \simeq \kappa^2 V(\phi), \quad (\text{A12})$$

$$-2\dot{H} \simeq \kappa^2 \left[ \left( 1 + 3\kappa^2 \theta(\phi) H^2 \right) \dot{\phi}^2 - \kappa^2 \theta_{,\phi} H \dot{\phi}^3 - 2\kappa^2 \theta(\phi) H \dot{\phi} \ddot{\phi} \right] , \quad (\text{A13})$$

$$\left( 1 + 3\kappa^2 \theta(\phi) H^2 \right) \ddot{\phi} + \left( 1 + 3\kappa^2 \theta(\phi) H^2 \right) 3H \dot{\phi} + \frac{3}{2} \kappa^2 \theta_{,\phi} H^2 \dot{\phi}^2 + V_{,\phi} \simeq 0 . \quad (\text{A14})$$

Using  $\{\epsilon, \delta_X, \delta_D\} \ll 1$  and Eq. (A13), we have

$$Q_s \simeq M_{\text{pl}}^2 (\delta_X + 6\delta_D) , \quad c_s^2 \simeq 1 , \quad (\text{A15})$$

and accordingly, the power spectrum given in Eq. (A11) can be approximately written as

$$\mathcal{P}_{\mathcal{R}} \simeq \frac{H^2}{8\pi^2 M_{\text{pl}}^2 (\delta_X + 6\delta_D)} . \quad (\text{A16})$$

- 
- [1] S. Bird, I. Cholis, J. B. Muñoz, Y. Ali-Haïmoud, M. Kamionkowski, E. D. Kovetz, A. Racanelli, and A. G. Riess, [Phys. Rev. Lett. \*\*116\*\*, 201301 \(2016\)](#).
  - [2] S. Clesse and J. García-Bellido, [Phys. Dark Universe \*\*15\*\*, 142 \(2017\)](#).
  - [3] M. Sasaki, T. Suyama, T. Tanaka, and S. Yokoyama, [Phys. Rev. Lett. \*\*117\*\*, 061101 \(2016\)](#).
  - [4] B. P. Abbott *et al.* (LIGO Scientific Collaboration and Virgo Collaboration), [Phys. Rev. X \*\*9\*\*, 031040 \(2019\)](#).
  - [5] P. Mróz, A. Udalski, J. Skowron, R. Poleski, S. Kozłowski, M. K. Szymański, I. Soszyński, L. Wyrzykowski, P. Pietrukowicz, K. Ulaczyk, D. Skowron, and M. Pawlak, [Nature \(London\) \*\*548\*\*, 183 \(2017\)](#).
  - [6] H. Niikura, M. Takada, S. Yokoyama, T. Sumi, and S. Masaki, [Phys. Rev. D \*\*99\*\*, 083503 \(2019\)](#).
  - [7] J. Scholtz and J. Unwin, [arXiv:1909.11090](#).
  - [8] A. Katz, J. Kopp, S. Sibiryakov, and W. Xue, [J. Cosmol. Astropart. Phys. \*\*12\*\* \(2018\) 005](#).
  - [9] H. Niikura *et al.*, [Nat. Astron. \*\*3\*\*, 524 \(2019\)](#).
  - [10] N. Aghanim *et al.* (Planck Collaboration), [arXiv:1807.06209](#).
  - [11] K. Kohri and T. Terada, [Phys. Rev. D \*\*97\*\*, 123532 \(2018\)](#).
  - [12] R. G. Cai, S. Pi, and M. Sasaki, [Phys. Rev. Lett. \*\*122\*\*, 201101 \(2019\)](#).
  - [13] R. G. Cai, S. Pi, S. J. Wang, and X. Y. Yang, [J. Cosmol. Astropart. Phys. \*\*05\*\* \(2019\) 013](#).
  - [14] K. Inomata and T. Nakama, [Phys. Rev. D \*\*99\*\*, 043511 \(2019\)](#).

- [15] S. Wang, T. Terada, and K. Kohri, [Phys. Rev. D \*\*99\*\*, 103531 \(2019\)](#).
- [16] Y. F. Cai, C. Chen, D. G. Wang, and S. F. Yan, [Phys. Rev. D \*\*100\*\*, 043518 \(2019\)](#)
- [17] W. T. Xu, J. Liu, T. J. Gao, and Z. K. Guo, [arXiv:1907.05213](#).
- [18] Y. Lu, Y. Gong, Z. Yi, and F. Zhang, [arXiv:1907.11896](#).
- [19] Y. F. Cai, X. Tong, D. G. Wang, and S. F. Yan, [Phys. Rev. Lett. \*\*121\*\*, 081306 \(2018\)](#).
- [20] C. Chen and Y. F. Cai, [J. Cosmol. Astropart. Phys. \*\*10\*\* \(2019\) 068](#).
- [21] G. Ballesteros, J. B. Jiménez, and M. Pieroni, [J. Cosmol. Astropart. Phys. \*\*06\*\* \(2019\) 016](#).
- [22] A. Y. Kamenshchik, A. Tronconi, T. Vardanyan, and G. Venturi, [Phys. Lett. B \*\*791\*\*, 201 \(2019\)](#).
- [23] S. Pi, Y. I. Zhang, Q. G. Huang, and M. Sasaki, [J. Cosmol. Astropart. Phys. \*\*05\*\* \(2018\) 042](#).
- [24] K. Inomata, M. Kawasaki, K. Mukaida, and T. T. Yanagida, [Phys. Rev. D \*\*97\*\*, 043514 \(2018\)](#).
- [25] Y. Tada and S. Yokoyama, [Phys. Rev. D \*\*100\*\*, 023537 \(2019\)](#).
- [26] J. Liu, Z. K. Guo, and R. G. Cai, [arXiv:1908.02662](#).
- [27] J. García-Bellido and E. R. Morales, [Phys. Dark Universe \*\*18\*\*, 47 \(2017\)](#).
- [28] C. Germani and T. Prokopec, [Phys. Dark Universe \*\*18\*\*, 6 \(2017\)](#).
- [29] H. Motohashi and W. Hu, [Phys. Rev. D \*\*96\*\*, 063503 \(2017\)](#).
- [30] J. M. Ezquiaga, J. García-Bellido, and E. R. Morales, [Phys. Lett. B \*\*776\*\*, 345 \(2018\)](#).
- [31] H. Di and Y. Gong, [J. Cosmol. Astropart. Phys. \*\*07\*\* \(2018\) 007](#).
- [32] G. Ballesteros and M. Taoso, [Phys. Rev. D \*\*97\*\*, 023501 \(2018\)](#).
- [33] I. Dalianis, A. Kehagias, and G. Tringas, [J. Cosmol. Astropart. Phys. \*\*01\*\* \(2019\) 037](#).
- [34] M. Drees and Y. Xu, [arXiv:1905.13581](#).
- [35] C. Fu, P. Wu, and H. Yu, [Phys. Rev. D \*\*100\*\*, 063532 \(2019\)](#).
- [36] K. N. Ananda, C. Clarkson, and D. Wands, [Phys. Rev. D \*\*75\*\*, 123518 \(2007\)](#).
- [37] D. Baumann, P. J. Steinhardt, K. Takahashi and K. Ichiki, [Phys. Rev. D \*\*76\*\*, 084019 \(2007\)](#).
- [38] T. L. Smith, E. Pierpaoli, and M. Kamionkowski, [Phys. Rev. Lett. \*\*97\*\*, 021301 \(2006\)](#).
- [39] L. Lentati *et al.*, [Mon. Not. R. Astron. Soc. \*\*453\*\*, 2576 \(2015\)](#).
- [40] C. J. Moore<sup>1</sup>, R. H. Cole<sup>1</sup>, and C. P. L. Berry, [Class. Quant. Grav. \*\*32\*\*, 015014 \(2015\)](#).
- [41] C. Germani and I. Musco, [Phys. Rev. Lett. \*\*122\*\*, 141302 \(2019\)](#).
- [42] C. Yuan, Z. Chen, and Q. Huang, [arXiv:1910.09099](#).